Optical Materials 121 (2021) 111606

Contents lists available at ScienceDirect

Optical Materials

journal homepage: www.elsevier.com/locate/optmat

Mn-doping-induced tunable bandgap and luminescence properties of SnO_2 nanoparticles grown by SILAR method

Muhammed Emin Güldüren [a,*], Ahmet Taşer [b], Harun Güney [c]

[a] Vocational School, Department of Electric and Energy, Agri Ibrahim Cecen University, Agri, Turkey
[b] Patnos Vocational School, Departments of Medical Services and Techniques, Agri Ibrahim Cecen University, Agri, Turkey
[c] Hınıs Vocational School, Departments of Medical Services and Techniques, Ataturk University, Erzurum, Turkey

ARTICLE INFO

Keywords:
Mn:SnO_2 thin films
XRD
SILAR
Bandgap and PL emission intensity tuning

ABSTRACT

In the present study, pure and Mn doped SnO_2 thin films were grown by performing successive ionic layer adsorption and reaction (SILAR) method on the glass substrates at room temperature. The fabricated thin films have been studied to assess the influence of Mn doping on structural, morphological, and optical properties of SnO_2 crystal lattice. The X-ray diffraction (XRD), Ultraviolet–visible spectrometer (UV–Vis), Energy dispersive X-ray analysis (EDAX), Scanning electron microscope (SEM), Raman, X-ray photoelectron spectroscopy (XPS), and Photoluminescence (PL) spectra measurements were conducted. After the XRD and SEM evaluations, it was found that the grown nanoparticles were in rutile type tetragonal structure of polycrystalline nature which was supported by Raman results. And, the surface morphologies were also observed to be affected from the varied concentrations of Mn doping. Besides, the EDAX evaluation confirmed the integration of Mn content next to Sn and O ions in the synthesized SnO_2 nanostructures by SILAR method. The UVi-vis analysis disclosed that the absorbance of the prepared thin films had a clear inclination to increase as doping concentration intensified. In addition to that, the optical investigations also uncovered the bandgap of SnO_2 nanocrystallines could be tuned from 2.61 eV to 2.00 eV by exposing them to the different levels of Mn ions. Furthermore, the Photoluminescence spectra evidently acknowledged the possibility of engineering optical characteristics by showing increased luminescent emission intensity values right after the introduction of impurities into the SnO_2 lattice. The XPS results further verified the manganese and tin valences existed in the produced thin films.

1. Introduction

In recent times, the fabrication and characterization of nanometric materials has acquired tremendous amount of interest owing to the fact that the material size can be profoundly associated with the material properties [1–4]. Correspondingly, the researches on semiconductor metal oxides (SMOs) such as (TiO_2, In_2O_3, Fe_2O_3, ZnO, V_2O_5, SnO_2, etc.) have been quite enticing due to their utilizations in nanodevices [2,5–7]. Among them, Tin oxide (SnO_2) is a noteworthy member of n-type SMOs with rutile tetragonal non-stoichiometric crystal structures. It also has a wide bandgap of 3.6 eV and large exciton binding energy (130 meV). Hence, it has been employed in various applications like catalysis, gas sensors, smart devices and optoelectronic devices due to its exceptional optical and electrical properties [1,3,8–10].

Impurity doped SnO_2 nanoparticles have been produced by several methods for instance chemical vapor deposition, spray pyrolysis, hydrothermal, sol-gel, thermal evaporation, RF magnetron sputtering, and so forth [1,4,9,11]. Whereas these methods are rather pricy for mass production of nanoparticles, successive ionic layer adsorption and reaction (SILAR) method has emerged to be one of the suitable and economic option to obtain nanoparticles in a simple manner. Also, the changes in morphology of the SMOs affect the physical properties of these nanostructures which have been noted to alter their efficiencies in photocatalytic activities. Accordingly, the selected deposition method is one of the most decisive factors for the end results of morphologic formations such as nanofibers, nanoparticles, nanoflowers, nanowires, nanorods, nanosheets, nanotubes, nanobelts, hollowspheres [3,4,12]. Therefore, this work is very significant since the studies on the structural as well as optical attributes of manganese (Mn) doped SnO_2 prepared by SILAR technique are still very minimal based on a recent literature survey in the web of science database, which brought only 4 results that include "SnO_2 SILAR" as keywords in their title.

* Corresponding author.
E-mail address: megulduren@agri.edu.tr (M.E. Güldüren).

https://doi.org/10.1016/j.optmat.2021.111606
Received 24 June 2021; Received in revised form 3 September 2021; Accepted 19 September 2021
Available online 25 September 2021
0925-3467/© 2021 Elsevier B.V. All rights reserved.

Furthermore, it is intriguing to realize that the transition metal (Cr, Ni, Mn, Co, Fe, etc.) doping has remarkable impact on optoelectronic characteristics of nanoscale SMOs such as optical bandgap and photoluminescence emission intensity [2]. In general, the previous studies used Mn as a doping agent concentrated on the magnetic bearings of Mn doped SnO_2 [8]. As a result, the reports related to Mn doping effect on the optoelectronic properties of SnO_2 require further researches. Besides, Mn ions could make good alternates for replacing Sn ion in SnO_2 crystal lattice since it possesses a large thermal solubility. Thus, it can help increasing the number of carriers and spins which could be beneficial for spintronic applications of SnO_2 thin films [13,14]. Herein, (0%, 0.5%, 1% and 2%) Mn doped SnO_2 nanoparticles have been successfully synthesized by the SILAR method for the first time as we know. Moreover, the influences of Mn doping on the structural, morphological and optical properties of the synthesized nanoparticles have been systematically explored.

2. Experimental

Mn doped SnO_2 nanocrystal thin films were produced onto glass slides by the successive ionic layer adsorption and reaction (SILAR) method. Before beginning the deposition, the glass slides were washed with diluted sulphuric acid (by 1/5 ratio), and then de-ionized (DI) water ultrasonically for 5 min each. Afterwards, the decontaminated glass slides were dried at 200 °C in an ashing furnace for 15 min. For the deposition, cationic and anionic precursors were prepared. Tin chloride ($SnCl_2 + 6H_2O$) was dissolved in 100 ml DI water to obtain 0.1 M cationic solution which divided into four 25 ml beakers after. Also, the anionic precursor was formed by adding sufficient amount of ammonia into DI water which stirred until pH 11 reached. To include the Mn as doping agent to the cationic precursors, 0.1 M manganese chloride ($MnCl_2$) solution was used in variable percentages (0.5%, 1%, and 2%) with respect to the beaker volume which contained pure SnO_2 solutions. Furthermore, the deposition was executed as shown in Fig. 1. This computer operated system contains two fundamental steps. First, the glass slides were first dipped into the cationic solution for 30 s at room temperature. Then, these slides were rinsed in the anionic solution for another 30 s which removes weakly attached ions from the substrate surfaces. Thus, one cycle of the SILAR deposition was completed as displayed in Fig. 1. And, for this particular thin film production, the deposition was run for 70 cycles. After the deposition, the produced samples were heat treated in the convection ashing furnace at 400 °C for 60 min to their final form. And, these samples were defined as pure SnO_2 and 0.5%, 1%, 2% Mn doped SnO_2 thin films, hereafter.

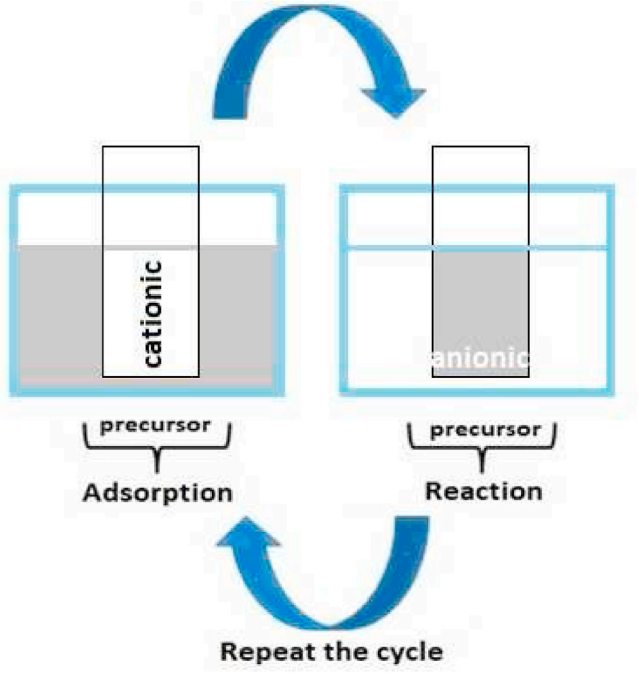


Fig. 1. Schematic representation of one cycle SILAR.

3. Results and discussion

Pure SnO_2 and SnO_2 thin films with different Mn doping concentrations were analyzed by XRD in order to define their crystal structures and related data such as peak positions (°2θ), full width at half maximum (FWHM), inter-planar distance (d), crystallite size (D), dislocation density (δ), and microstrain (ϵ). XRD diffraction peaks were given in Fig. 2. The diffraction peaks of pure SnO_2 sample appear to be composed of four distinct peaks at 26.63°, 33.9°, 37.95°, and 51.8° which can be indexed to the (110), (101), (200) and (211) lattice planes. These XRD peaks have shown that the produced SnO_2 nanostructures are rutile tetragonal crystal structures of SnO_2 with P42/mnm symmetry which found to be compatible with JCPDS card number 41–1445 [2,9]. The preferred growth orientation for all SnO_2 samples was noted to be (110) as shown in Fig. 2. And, the preferred orientation for SnO_2 nanocrystals has been reported to be located at (110) plane according to the previous work [9,11,12]. Besides, formation of impurity peaks were also observed to occur in addition to the peaks for pure SnO_2 as Mn dopant concentration increased. In Fig. 2, two soft peaks marked with star (*) signs were displayed, which thought to be the diffraction peaks of the MnO_2 structure, derived from Mn impurity atoms by the replacement of Sn^{4+} (71 p.m.) with Mn^{4+} (54 p.m.) ion [15,16]. The XRD patterns also reveal the presence of variations in the peak sharpness which might be another effect originated from the well assimilation of Mn^{4+} ions at the SnO_2 lattice sites [8,9].

The variations in the inter-planar distance (d) and the lattice constant (a) values have been calculated based on the XRD peak (110) of all samples by employing the formulas below [17],

$$n\lambda = 2d\sin\theta \tag{1}$$

$$d = \frac{a}{\sqrt{(h^2 + k^2 + l^2)}} \tag{2}$$

where n equals to 1, λ is the wavelength of the X-ray beam ($\lambda = 1.5406$), θ is the diffraction angle of the preferred plane orientations, and (hkl) are the Miller indices. In Table 1, it can be seen that the d values for the preferred orientation (110) initially increased slightly with 0.5% Mn

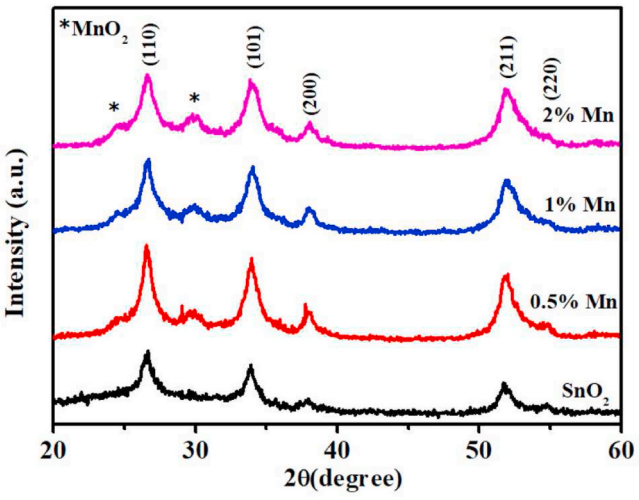


Fig. 2. The XRD spectra pure and Mn doped SnO_2 thin films.

Table 1
Eg, peak positions ($^{o}2\theta$), FWHM, inter-planar distance (d), the particle sizes (D), the dislocation density (δ), the microstrain (ε), and the lattice constant (a) values of the pure and Mn doped SnO_2 thin films.

Sample name	Eg (eV)	Pos. (°2θ)	FWHM (°2θ)	*d*-spacing (Å)	*D* (nm)	δ (10^{13} cm^{-2})	ϵ (10^{-2}%)	*a* (Å)
SnO	2.61	26.63	1.032	3.345	14.42	48.09	0.25	4.7301
0.5% Mn	2.42	26.56	1.141	3.353	13.04	58.80	0.28	4.7424
1% Mn	2.19	26.71	1.002	3.335	14.85	45.32	0.24	4.7162
2% Mn	2.00	26.65	0.908	3.342	16.39	37.22	0.22	4.7266

doping, and then it decreased as Mn doping concentration increased to 1% and 2%. And, the tabulated values of d are in accordance with the inter-planar spacing of the (110) [18]. Furthermore, in Table 1, the lattice constants were given as 4.7301, 4.7424, 4.7162 and 4.7266 Å corresponding to the pure SnO_2, (0.5%, 1% and 2%) Mn doped SnO_2, respectively. The obtained lattice constants concurs well with the values of (a) for tin oxides found in the presented JCPDS card ($a = 4.7382$ Å). These occurrences in d and a values may be explained by the distortions arisen from the increased volume of manganese doping in the SnO_2 lattices. In addition to that, this shrinkage in the inter-planar distances and the lattice constants of the produced SnO_2 samples with the increase of Mn doping percentages may indicate the occupied interstitial positions by Mn^{4+} ions as their ionic sizes are smaller than the host, as well as substitution of Sn^{4+} ions by the same dopants [1,8,9,18].

In Table 1, the crystalline size *(D)*, dislocation density *(δ)* and lattice strain *(ε)* of all the samples were calculated using the given formulas below [18].

$$D = \frac{0,9\lambda}{\beta\, cos\theta} \tag{3}$$

$$\delta = \frac{1}{D^2} \tag{4}$$

$$\varepsilon = \frac{\beta\, cos\theta}{4} \tag{5}$$

where λ is the wavelength of X-ray radiation, and β is the full width at half maximum (FWHM) of the peaks at the Bragg diffraction angle θ in degree. In Table 1, the crystallite sizes for (110) peak were disclosed to be 14.42 nm, 13.04 nm, 14.85 nm and 16.39 nm for 0%, 0.5%, 1%, and 2% Mn doping levels in the grown SnO_2 nanocrystallines. It is clearly recognized that the D values first decreased at the presence of lower Mn content (0.5%) which might be induced by the increased nucleation centers [19]. And, they also showed increment as the doping rate went up to 2%, which may be induced by the scattering of Mn ions into the SnO_2 lattices [20]. On the other hand, as illustrated in Table 1, the dislocation density and the grain size can be acknowledged to be inversely related to the crystallite sizes. Table 1 displays that the δ values decreased from 48.09 (10^{13} cm^{-2}) to 37.22 (10^{13} cm^{-2}), and the ε data exhibited reduction from 0.25 (10^{-2}%) to 0.22 (10^{-2}%) as well. Therefore, these facts can also be interpreted as lower δ and ε may help enhancing the crystallinity of the thin films [18–20].

Fig. 3 shows the SEM images of the synthesized pure and (0.5%, 1% and 2%) Mn doped SnO_2 nanoparticles by SILAR method. Fig. 3 (a, c, e, g) display 25,000 times magnified looks of the produced SnO_2 thin films. It can be seen that these particles were nonuniform well defined crystals with dominant spherical shapes as displayed in Fig. 3. And, Mn doped SnO_2 nanostructures were detected to possess slightly bigger or smaller crystallite sizes than that of pure tin oxide sample which are in tune with the XRD data given in Table 1. In addition to that, the accumulation of nanoparticles was notably increased after variable amounts of Mn ions introduced to the system. The happening of variable grain sizes in the preferred plane orientation was spurred due to the increment in Mn doping concentration in SnO_2 nanostructures as reported in the XRD analysis. And, Fig. 3 (e, g) demonstrates united grains which formed nanoflower like clusters ultimately due to the increased presence of impurity dopings in the SnO_2 crystal lattices [1,8,12]. Furthermore, Fig. 3 (b, d, f, h) exposes the elemental configuration of the deposited Mn:SnO_2 nanocompounds which was carried out by Energy Dispersive X-ray measurement. The EDX spectrum assuredly confirms the existence of Sn, O, and Mn elements on the surface of the prepared samples by the cost-effective SILAR method. And, the absence of other impurity atoms was also confirmed by the EDX analysis.

In Fig. 4 (a), transmittance spectras of the grown SnO_2 thin film samples were plotted by performing Ultraviolet–visible spectroscopy in the range of 300–1100 nm at room temperature. The transmittance of the pure SnO_2 sample was found to be around 65% (at 1100 nm). Besides, the transmittance value of pure tin oxide in the focused region (300 nm–1100 nm) started to decrease over the entire spectrum as soon as doping began. And, it kept decreasing as low as ~25% (at 1100 nm) while the doping concentration increased in the SnO_2 crystal lattices. This may suggest that the increase in Mn doping concentration caused to improve the degenerate (metallic) nature of the prepared SnO_2 nanostructures, which can generate intense light absorption. Also, the samples with higher dopant rates were noticed to turn brownish in color after heat treatment, and they appeared to be less transparent to the naked eye compared to the pure SnO_2 sample. In addition to that, the decrease in transmittance values can also be explained by the disorders and defects in the SnO_2 nanocrystallite system due to the inserted impurity atoms to the lattice, which are mentioned in the XRD data at Table 1. Similar effects of Mn doping over transmittance characteristics of produced nanostructures were reported in the previous studies as well [21–23].

Fig. 4 (b) shows the absorbance spectra of the SnO_2 thin films based on the wavelengths ranging from ultraviolet (UV) to infrared (IR) region, which is applied to figure out the optical bandgap energy (E_g). The absorption edge for pure SnO_2 thin film was observed to shift towards lesser energy levels with building Mn composition, and this edge might be an indication of the transfer of photo excited electrons from valence band to conduction band due to the introduced impurities by the SILAR method. In Fig. 4 (b), it can be seen that the absorbance, which is known to be affected by material aspects like impurity centers, oxygen vacancies, surface uniformity, etc., tends to increase with the amplifying amount of manganese content in the SnO_2 samples [2,5,11]. In Fig. 4 (c) and Table 1, the E_g values of the grown SnO_2 nanostructures were presented by applying the Tauc relation;

$$\alpha = \frac{Absorbance}{t} \tag{6}$$

$$(\alpha h\upsilon) = A\left(h\upsilon - E_g\right)^n \tag{7}$$

where α, $h\upsilon$, t, and A quantities are used to refer to the absorption coefficient, the incident photon energy, the thickness, and an energy-independent constant, respectively. And, n is equal to 1/2 for direct bandgap semiconductor materials. The E_g values were found to be 2.61 eV, 2.42 eV, 2.19 eV, and 2.00 eV for pure SnO_2 and (0.5%, 1% and 2%) Mn doped SnO_2 samples consecutively, which is compatible with previous work [2,6,24]. This observed bandgap narrowing (red shift) may be ascribed to the successful ion substitutions between Mn^{4+} doping agents and Sn^{4+} sites in the SnO_2 lattices where the sp–d exchange

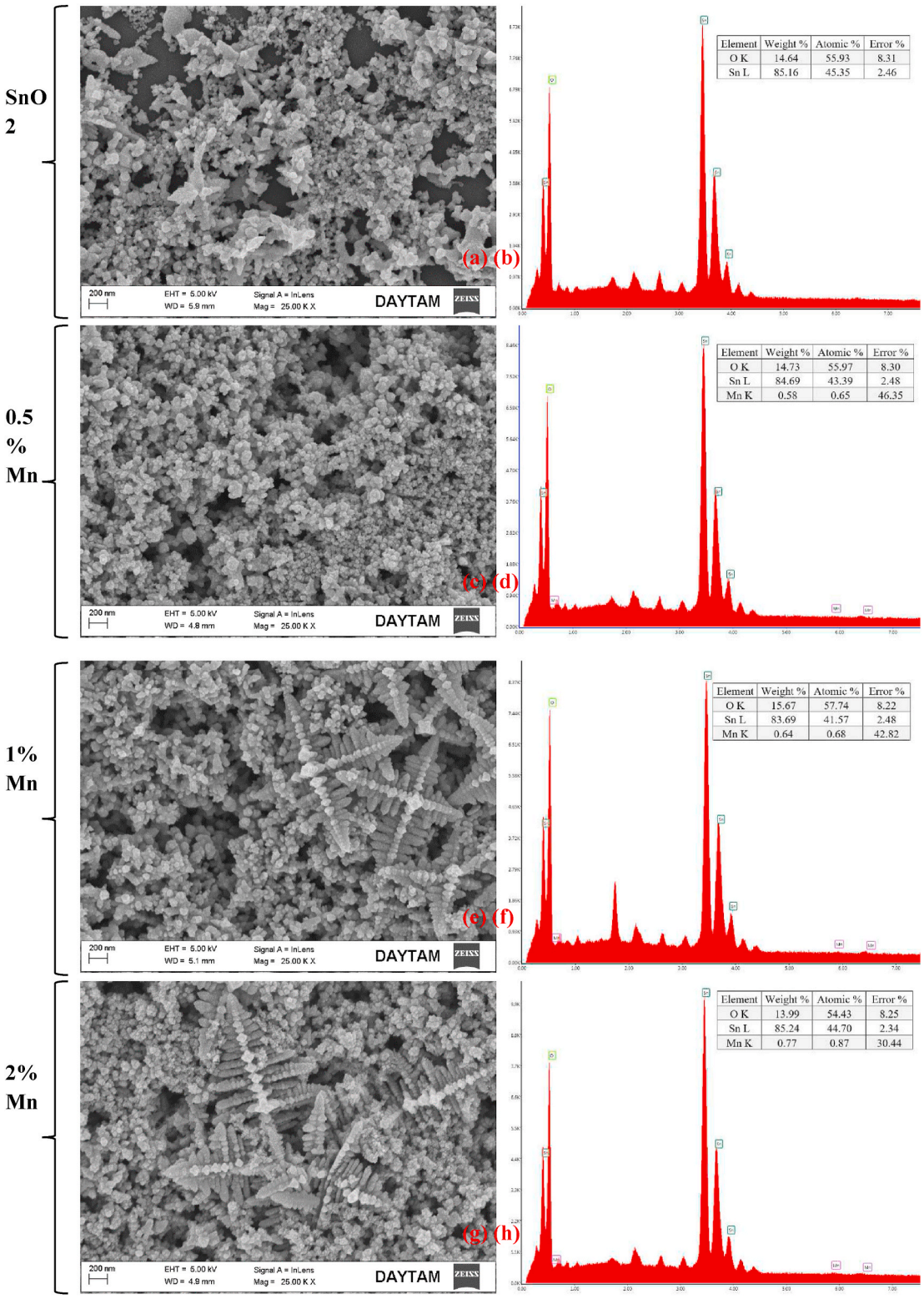


Fig. 3. (a, c, e, g) SEM images of pure and Mn doped SnO_2 thin films, (b, d, f, h) EDAX analysis of pure and Mn doped SnO_2 thin films.

interactions among the conduction band (CB) and valence band (VB) edges [11,24]. Besides, this alteration in the SnO_2 bandgaps confirms the presence of crystal deteriorations which may boost the production of some impurity levels close to the conduction band. Accordingly, this will prompt the Fermi-level of the grown SnO_2 thin films to shift, and hence create new donor levels in the forbidden band gap. Therefore, these newly formed band layers could merge with the CB which leads to shortening of the bandgaps in the prepared SnO_2 samples [6,11,19]. Also, the red shift in the bandgap values might be due to the modified structural parameters as shown in Table 1, which may lead to size induced quantum confinement effect [11]. According to this effect, the variations in crystallite size affect the optical bandgap energy of materials. In the obtained XRD parameters, it was observed that the crystallite size changed due to the existence of impurities, which may be

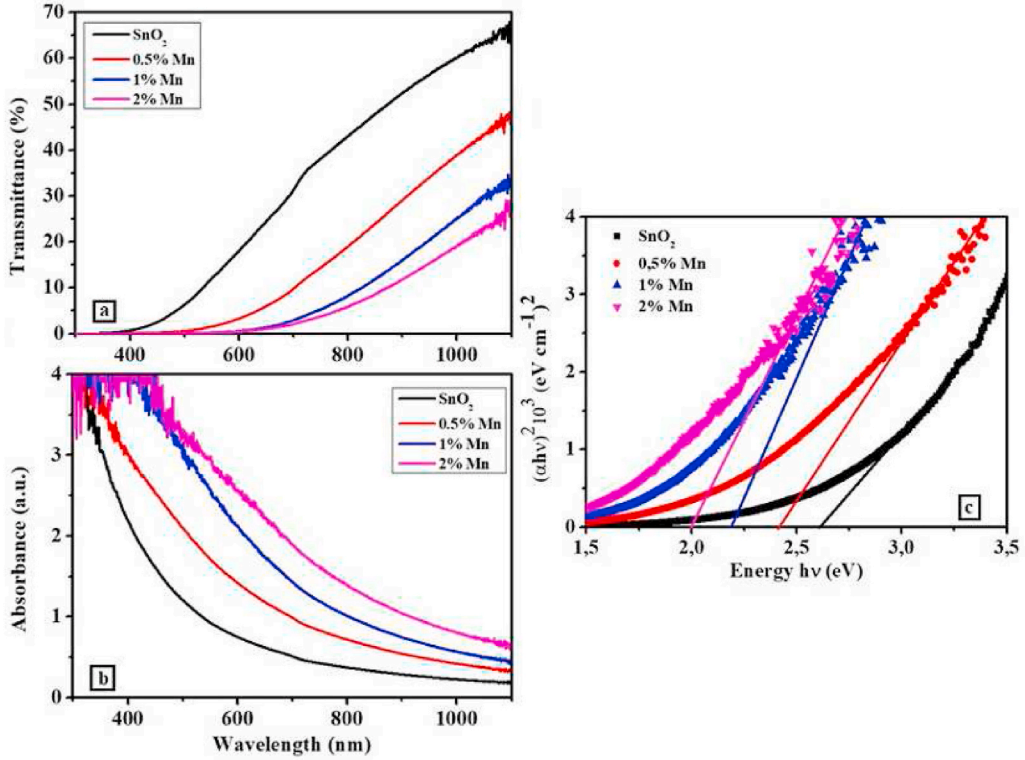


Fig. 4. UV–Visible (a) transmittance, (b) absorbance and (c) Tauc's Plots for band gap energy spectra of pure and Mn doped SnO_2 thin films.

another reason for the narrowed optical bandgaps of SnO_2 nanostructures. Hence, it can be said that the crystalline defects, presented in the XRD data, were generated by Mn content, and the impurity doping can effectively tailor the optical bandgap for optoelectronic applications [6,9,19].

Fig. 5 demonstrates the room temperature photoluminescence spectra (PL) of the synthesized SnO_2 samples having different Mn concentrations (0%, 0.5%, 1%, and 2%). The PL spectra of all the grown SnO_2 nanoparticles display rather close peak positions in the wavelength range of 350 nm–700 nm. Two distinct emission peaks were noticed to be located at 498 nm (2.48 eV), and 553 nm (2.24 eV). And, these emission spikes correspond to the defect related emissions which were the cyan (485–500 nm) and green emission (500–565 nm), respectively. It is curious to mark that the emission intensity of these bands increased as soon as the Mn dopants introduced, and the intensity of 0.5% Mn doped sample was enhanced to around eight folds of the magnitude of the pure SnO_2 sample. Thus, it can be said that inserting Mn ions is a potent way to amend the luminescent characteristic of SnO_2 semiconductor films. However, this trend was not continuous for all doping levels. Although, the higher doping levels (%1 and 2%) also showed stronger emission intensities compared to the pure SnO_2 sample, the PL peak of lowest (0.5%) Mn doped SnO_2 possessed the most intense peak in Fig. 5. This observed behavior could be related to reshaped bandgap structure and increase in oxygen vacancies as a result of varied quantity of Mn ions cumulated in the lattice system [2,6]. Moreover, there is a clear shift that occurred in the emission peaks toward the lower wavelengths upon 0.5% Mn doping as shown in Fig. 5. This effect might be accredited to the integration of impurities in SnO_2 which could have modified the internal disorganization as well as the locations of oxygen vacancies, and their placement over the thin film surfaces [2,6,11].

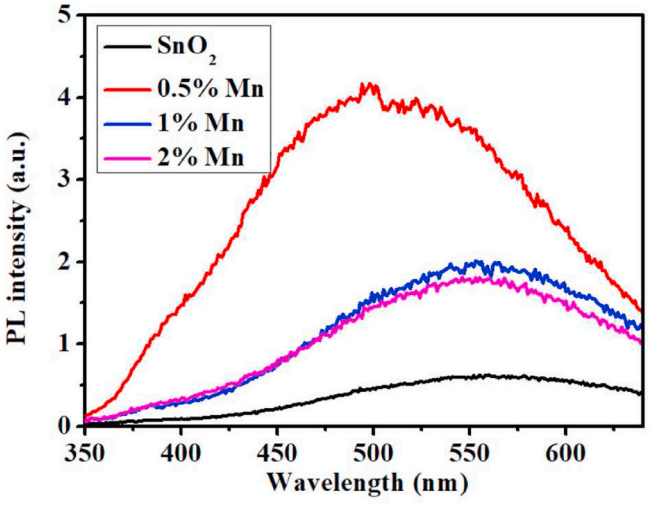


Fig. 5. The PL spectroscopy of pure and Mn doped SnO_2 thin films.

Raman measurement is a technique based on the analysis of the inelastically scattered photons from a material medium, which produced by the interaction of light with crystal vibrations. During the Raman spectroscopy measurements, the energy shift between incident and inelastically scattered light is usually studied. In addition to that, Raman spectroscopy is a capable and non-destructive technique to examine defects within the crystal structure and defects in semiconductors with doping atoms. It yields important information about the local structure changes in the SnO_2 crystal lattice of the additive ions caused by incompatibility [8,9]. In Fig. 6, the Raman spectroscopy measurements were conducted to verify the position of Mn doping atoms in the SnO_2 crystal structures, and to understand the effect on vibration properties of SnO_2 semiconductors. Tin oxide is well known to have a tetragonal structure with two tin atoms and four oxygen atoms per unit cell, with point group D_{4h}^{14} and space group $P4_2/mnm$. It consists of six-unit cell atoms giving a total of 18 vibrational modes in the first Brillouin Zone. Their presentation of vibration modes in the center of the Brillouin region is given as [2,25]:

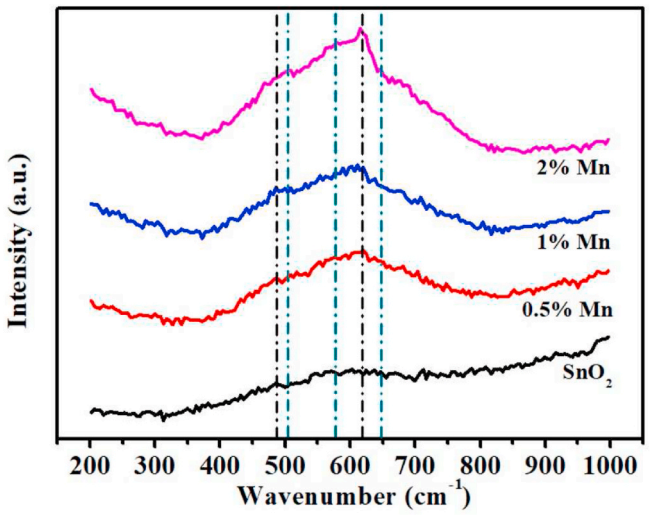


Fig. 6. The Raman spectra of pure and Mn doped SnO_2 thin films.

presence of basic elements of tin, manganese, carbon and oxygen can seen in the XPS spectra as shown in Fig. 7 (a). Two symmetrical spin-trajectory pairs, $Sn3d_{5/2}$ and $Sn3d_{3/2}$, of the core levels corresponding to Sn3d were noted in the XPS spectrum. These peaks reveal that the prepared samples have a valence state of Sn^{4+} [1,6,28]. In Fig. 7 (b), the XPS peaks of the 2% Mn doped SnO_2 sample corresponds to the core levels of Mn $2p_{3/2}$ and $2p_{1/2}$ and O 1s which can be associated with the characteristic MnO and it proves the existence of Mn^{4+} dopant ions [4,7]. Additionally, C1s peak was observed in the XPS spectrum due to the unexpected hydrocarbon coming from the XPS device itself.

4. Conclusion

To the best of our knowledge, a series of pure and Mn doped SnO_2 thin films were successfully fabricated by employing the SILAR method for the first time. It is concluded from the structural and morphological analysis carried out by XRD, EDAX, SEM, Raman and XPS that the addition of Mn into the SnO_2 crystal lattices had a substantial influence over the relevant characteristics of the produced thin films. The X-ray diffraction data calculations suggested that impurity doping had a strong impact affecting the crystallite size, dislocation density, and microstrain of the SnO_2 samples with preferred (110) plane orientation.

$$\Gamma = \Gamma_1^+(A_{1g}) + \Gamma_2^+(A_{2g}) + \Gamma_3^+(B_{1g}) + \Gamma_4^+(B_{2g}) + \Gamma_5^-(E_g) + 2\Gamma_1^-(A_{2u}) + 2\Gamma_4^-(B_{1u}) + 4\Gamma_5^+(E_u) \quad (8)$$

A_{1g}, B_{1g}, B_{2g} and E_g modes are Raman active, while A_{2u} and E_u are infrared active. Raman spectra of pure SnO_2 and Mn-doped SnO_2 thin films at room temperature are shown in Fig. 6. It is interesting to note that the most intense Raman peak found at 624 cm^{-1} intensified by substituting Mn ions into the SnO_2 lattice, which can be attributed to the A_{1g} vibrational mode. Also, another main peak for pristine SnO_2 represented by dashed black lines (at 485 cm^{-1}) may be attributed to the vibrational mode E_g. These peaks confirm that SnO_2 thin films have the properties of tetragonal rutile structure [3,11,25]. Furthermore, the peaks shown with green dashed lines were located at 508 cm^{-1}, 580 cm^{-1}, and 646 cm^{-1}. And, all these peaks are in good agreement with the Raman peaks of birnessite-type MnO_2 compounds which have been previously reported to be found at 500–510, 575–585 and 625–650 cm^{-1} [12,26,27].

The oxidation state of pure and Mn doped SnO_2 thin films, their surface chemical components and the presence of additives were systematically investigated by X-ray photoelectron spectroscopy (XPS). The

This alterations caused by Mn dopants was also reflected in SEM studies owing to the fact that the occurrences of different grain sizes and shapes in the SnO_2 nanostructures. The absorbance and transmittance spectras were noticed to be inversely proportioned to each other as a response to the changing Mn doping concentrations. Besides, the UV–vis analysis provided that the optical bandgap was reduced from 2.61 eV to 2.00 eV due to the sp–d exchange interactions and crystal defects. And, the PL spectra suggested that the variations in Mn doping percentages in the SnO_2 nanocrystals can be taken advantage of when it comes to controlling the luminescent emission intensity. Raman and XPS confirmed that Sn^{4+} ions were successfully substituted by Mn^{4+} ions into the host SnO_2 matrix without any impurity phases. In the light of these results, it can be remarked that these SnO_2 thin films emerge as promising candidates to be utilized in optoelectronic nanodevices due to their tunable structural and optical properties which can also be beneficial to many other researches.

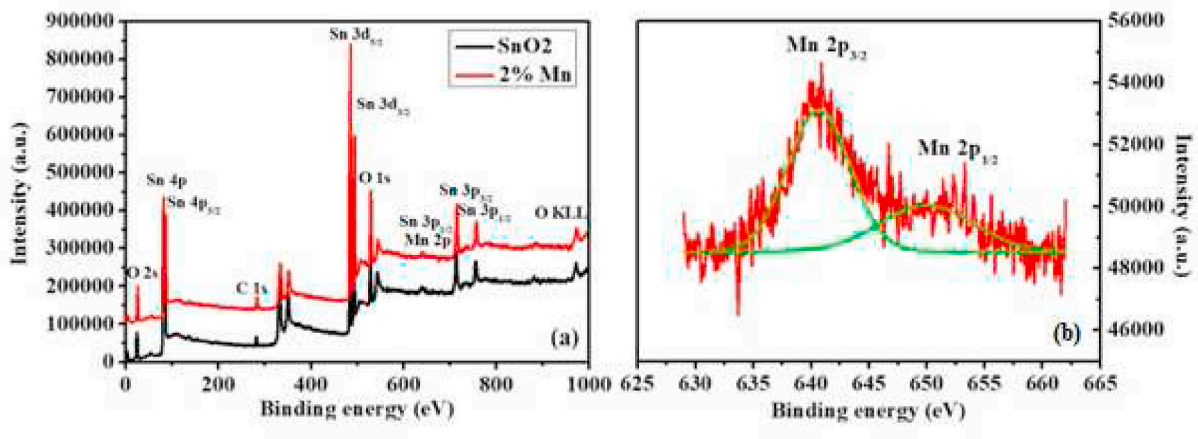


Fig. 7. The XPS spectra of pure and Mn doped SnO_2 thin films.

Author agreement statement

We the undersigned declare that this manuscript is original, has not been published before and is not currently being considered for publication elsewhere.

CRediT authorship contribution statement

Muhammed Emin Güldüren: Conceptualization, Funding acquisition, Data curation, Writing – original draft, Formal analysis, Conception and design of study, acquisition of data, analysis and/or interpretation of data, Drafting the manuscript, revising the manuscript critically for important intellectual content, Approval of the version of the manuscript to be published. **Ahmet Taşer:** Conceptualization, Funding acquisition, Data curation, Writing – original draft, Formal analysis, Conception and design of study, acquisition of data, analysis and/or interpretation of data, Drafting the manuscript, revising the manuscript critically for important intellectual content, Approval of the version of the manuscript to be published. **Harun Güney:** Conceptualization, Funding acquisition, Data curation, Writing – original draft, Formal analysis, Conception and design of study, acquisition of data, analysis and/or interpretation of data, Drafting the manuscript, revising the manuscript critically for important intellectual content, Approval of the version of the manuscript to be published.

Declaration of competing interest

The authors declare that they have no known competing financial interests or personal relationships that could have appeared to influence the work reported in this paper.

Acknowledgments

The authors thank Agri Ibrahim Cecen University for financial support of the study (Project no: MYO-21-003).

References

[1] Seher Tas Anli, Mehmet Faruk Ebeoglugil, Erdal Celik, Effect of dopant elements on structure and morphology of SnO_2 nanoparticles, Journal of the Australian Ceramic Society 56 (2) (2020) 403–411.
[2] K. Srinivas, M. Vithal, B. Sreedhar, M. Manivel Raja, P. Venugopal Reddy, Structural, optical, and magnetic properties of nanocrystalline Co doped SnO_2 based diluted magnetic semiconductors, J. Phys. Chem. C 113 (9) (2009) 3543–3552.
[3] Wenzhong Wang, Congkang Xu, Guanghou Wang, Yingkai Liu, Changlin Zheng, Synthesis and Raman scattering study of rutile SnO_2 nanowires, J. Appl. Phys. 92 (5) (2002) 2740–2742.
[4] Syed Shaheen Shah, Md Abdul Aziz, Amar Kamal Mohamedkhair, Mohammed Ameen Ahmed Qasem, Abbas Saeed Hakeem, Mazen Khaled Nazal, Zain Hasan Yamani, Preparation and characterization of manganese oxide nanoparticles-coated Albizia procera derived carbon for electrochemical water oxidation, J. Mater. Sci. Mater. Electron. 30 (17) (2019) 16087–16098.
[5] Akanksha Gupta, Prashant Kumar, Adish Tyagi, Ravinder Kumar, Ashwani Kumar, Prashant Singh, R.P. Singh, Vinod Kumar, Facile synthesis of N-doped SnO_2 nanoparticles: a cocatalyst-free promising photocatalyst for hydrogen generation, Chemistry 5 (26) (2020) 7775–7782.
[6] Ateeq Ahmed, M. Naseem Siddique, T. Ali, P. Tripathi, Defect assisted improved room temperature ferromagnetism in Ce doped SnO_2 nanoparticles, Appl. Surf. Sci. 483 (2019) 463–471.
[7] Yongming Sun, Xianluo Hu, Wei Luo, Fangfang Xia, Yunhui Huang, Reconstruction of conformal nanoscale MnO on graphene as a high-capacity and long-life anode material for lithium ion batteries, Adv. Funct. Mater. 23 (19) (2013) 2436–2444.
[8] Syed Mansoor Ali, Jan Muhammad, Syed Tajammul Hussain, Shahzad Abu Bakar, Muhammad Ashraf, Study of microstructural, optical and electrical properties of Mg dopped SnO thin films, J. Mater. Sci. Mater. Electron. 24 (7) (2013) 2432–2437.
[9] S. Vadivel, G. Rajarajan, Effect of Mg doping on structural, optical and photocatalytic activity of SnO_2 nanostructure thin films, J. Mater. Sci. Mater. Electron. 26 (5) (2015) 3155–3162.
[10] B. Liu, C.W. Cheng, R. Chen, Z.X. Shen, H.J. Fan, H.D. Sun, Fine structure of ultraviolet photoluminescence of tin oxide nanowires, J. Phys. Chem. C 114 (8) (2010) 3407–3410.
[11] Ameer Azam, Arham S. Ahmed, Sami S. Habib, A.H. Naqvi, Effect of Mn doping on the structural and optical properties of SnO_2 nanoparticles, J. Alloys Compd. 523 (2012) 83–87.
[12] Hui Xia, Yu Wang, Jianyi Lin, Li Lu, Hydrothermal synthesis of MnO_2/CNT nanocomposite with a CNT core/porous MnO_2 sheath hierarchy architecture for supercapacitors, Nanoscale research letters 7 (1) (2012) 1–10.
[13] X.G. Chen, W.W. Li, J.D. Wu, J. Sun, K. Jiang, Z.G. Hu, J.H. Chu, Temperature dependence of electronic band transition in Mn-doped SnO_2 nanocrystalline films determined by ultraviolet-near-infrared transmittance spectra, Mater. Res. Bull. 47 (1) (2012) 111–116.
[14] Y.S. Wang, P. John Thomas, P. O'Brien, Optical properties of ZnO nanocrystals doped with Cd, Mg, Mn, and Fe ions, J. Phys. Chem. B 110 (43) (2006) 21412–21415.
[15] S. Devaraj, N. Munichandraiah, Effect of crystallographic structure of MnO_2 on its electrochemical capacitance properties, J. Phys. Chem. C 112 (11) (2008) 4406–4417.
[16] Yang Yu, Xuan Wang, Xiaoming Wang, Li Xue, Ling Weng, Xiaorui Zhang, Enhanced energy storage efficiency in PVDF based composite films using MnO_2 nano-fillers, J. Mater. Sci. Mater. Electron. 31 (21) (2020) 18336–18343.
[17] Cullity, Bernard Dennis, Elements of X-Ray Diffraction, Addison-Wesley Publishing, 1956.
[18] Güven Turgut, E. Sonmez, Serdar Aydın, Refik Dilber, U. Turgut, The effect of Mo and F double doping on structural, morphological, electrical and optical properties of spray deposited SnO_2 thin films, Ceram. Int. 40 (8) (2014) 12891–12898.
[19] Allag Abdelkrim, Saâd Rahmane, Ouahab Abdelouahab, Nadjate Abdelmalek, Gasmi Brahim, Effect of solution concentration on the structural, optical and electrical properties of SnO_2 thin films prepared by spray pyrolysis, Optik 127 (5) (2016) 2653–2658.
[20] Xiaohua Zhong, Baoping Yang, Xiaoliang Zhang, Junhong Jia, Gewen Yi, Effect of calcining temperature and time on the characteristics of Sb-doped SnO_2 nanoparticles synthesized by the sol–gel method, Particuology 10 (3) (2012) 365–370.
[21] K. Gopinadhan, Subhash C. Kashyap, Dinesh K. Pandya, Sujeet Chaudhary, High temperature ferromagnetism in Mn-doped SnO_2 nanocrystalline thin films, J. Appl. Phys. 102 (11) (2007) 113513.
[22] H. Kimura, T. Fukumura, M. Kawasaki, K. Inaba, T. Hasegawa, H. Koinuma, Rutile-type oxide-diluted magnetic semiconductor: Mn-doped SnO_2, Appl. Phys. Lett. 80 (1) (2002) 94–96.
[23] E. Elangovan, M.P. Singh, M.S. Dharmaprakash, K. Ramamurthi, Some physical properties of spray deposited SnO_2 thin films, J. Optoelectron. Adv. Mater. 6 (1) (2004) 197–203.
[24] S. Kesava Pandian, K. Karthik, K. Sureshkumar, N. Victor Jaya, Effect of Mn-doping on structural, optical, and dielectric properties of SnO_2 nanoparticles by coprecipitation method, Mater. Manuf. Process. 27 (2) (2012) 130–134.
[25] A. Dieguez, A. Romano-Rodrıguez, A. Vila, J.R. Morante, The complete Raman spectrum of nanometric SnO_2 particles, J. Appl. Phys. 90 (3) (2001) 1550–1557.
[26] A. Ogata, R. Shinichi Komaba, Baddour-Hadjean, J.-P. Pereira-Ramos, N. Kumagai, Doping effects on structure and electrode performance of K-birnessite-type manganese dioxides for rechargeable lithium battery, Electrochim. Acta 53 (7) (2008) 3084–3093.
[27] C. Julien, M. Massot, R. Baddour-Hadjean, S. Franger, S. Bach, J.P. Pereira-Ramos, Raman spectra of birnessite manganese dioxides, Solid State Ionics 159 (3–4) (2003) 345–356.
[28] Shaidatul Najihah Matussin, Ai Ling Tan, Mohammad Hilni Harunsani, Mohammad Akbar, Moo Hwan Cho, Mohammad Mansoob Khan, Effect of Ni-doping on properties of the SnO2 synthesized using Tradescantia spathacea for photoantioxidant studies, Mater. Chem. Phys. 252 (2020) 123293.